Numerical Analysis for Motion Response of Modular Floating Island in Waves

Hyo-Jin Park [1], Jeong-Seok Kim [2] and Bo Woo Nam [3]

[1]Graduate student, Department of Naval Architecture and Ocean Engineering, Seoul National University, Seoul, Korea
[2]Junior Researcher, Eco-friendly Ocean Development Research Division,
Korea Research Institute of Ships & Ocean Engineering, Deajeon, Korea
[3]Assistant Professor, Department of Naval Architecture and Ocean Engineering, Seoul National University, Seoul, Korea

ABSTRACT: *In recent years, modular-type floating islands have been considered as a promising option for future ocean space utilization. A modular floating island consists of a number of standardized pontoon-type modules and connectors between them. In this study, the motion responses of a modular floating island in waves was investigated based on frequency-domain numerical analysis. The numerical method is based on the potential flow theory and adopts a higher-order boundary element method with Green's function. First, motion RAOs were directly compared with the model test data by reference to validate the present numerical method. Then, numerical investigations were conducted to analyze the motion characteristics of the floating island by considering various modules shapes and arrangements. It was found that motion responses were reduced in a single central module compared to when divided central modules were used. Finally, the effect of modular arrangement on the motion responses in irregular waves was discussed. It was confirmed that multiple-layer outer modules are more effective in calming the central module than using single-layer outer modules, except under very long period conditions.*

1. Introduction

The demand for ocean space utilization is rising because of the recent rise in sea level and population density in coastal regions. As a strategy to exploit the ocean space, expanding land space through land reclamation has been widely adopted. However, in terms of environmental protection and economic feasibility, floating islands have been actively studied (Yeh et al., 2015; Lu et al., 2015). In Japan, floating islands have been used for airports and fuel storage facilities because floating island technology can minimize environmental damage compared to the coastal reclamation development (Wang and Tay, 2011). In South Korea, floating island structures have been employed as maritime recreational amenities in combination with waterfront infrastructure projects. Furthermore, floating islands are used as salmon farming facilities in Canada, Chile, Norway and the United States. Recently in Europe, research projects on multi-purpose very large offshore structures for dwelling, fishing, energy generation and storage functions have been launched and related research is being conducted.

Very large floating structures (VLFS) for floating islands have been generally classified into semi-submersible and pontoon types. A semi-submersible VLFS has an topside platform above the water surface, which is suitable for use in the open ocean. On the other hand, a pontoon type VLFS has a floating platform on the water surface, which is appropriate for mild seas (Wang and Tay, 2011). Furthermore, a pontoon type VLFS has the advantages of simple structure, good stability, low manufacturing and maintenance costs, and easy repair (Lamas-Pardo et al., 2015). So far, many studies on the integrated pontoon-type VLFS have been conducted focusing on structural safety evaluation considering the hydroelastic response (Kashiwagi, 1998; Kim et al., 2014). This is because the structural deformation of the pontoon-type VLFS is rather substantial owing to the small draft compared to the length.

Some studies have been conducted regarding the modular floating island, which links multiple modules through connectors. Watanabe et al. (2004) pointed out that most floating islands, including the integrated type, need to be manufactured by combining a number of standardized modules in order to overcome difficulties in

manufacturing, transportation, and installation. This implies that an integrated floating island can be changed into the modular floating island by introducing the appropriate connectors. Wu et al. (1993) and Riggs et al. (2000) performed numerical analysis on the hydroelastic response of a semi-submersible VLFS composed of five modules. Fu et al. (2007) reported the numerical results that the hydroelastic response of the integrated floating island can be changed as the pontoon type module was connected via flexible connectors. Gao et al. (2011) showed the hydroelastic response and load of a pontoon- type VLFS are reduced by applying a hinge connector that allows some floater movement under short wave conditions. This suggests that the modular method using flexible connectors, which allows some relative movement between modules, has an advantage over the integral method using rigid connectors to restrain the VLFS in terms of hydroelastic response and load.

Recently, active research is now being performed to utilize pontoon-type VLFS in the form of a modular floating island. Zhang et al. (2015) conducted a numerical study on a marine airport in which two to five pontoon modules were connected via flexible connectors. In Europe, a modular floating island composed of 87 pontoon modules was proposed through the "Space@Sea Project". The motion response of a modular floating island was described by Waals et al. (2018) who performed a series of model test. Otto et al. (2019a) conducted a potential flow-based numerical analysis in the frequency domain. Otto et al. (2019b) evaluated the motion response of the module and the load acting on the connector with different dimensions of the floating island, and demonstrated that module size has a significant effect on the motion response of a modular floating island. However, their study did not closely examine the effects of module arrangement on the motion response and load of the floating island.

Numerical models for a modular floating island can be divided into a rigid module & flexible connector model and a flexible module & flexible connector model depending on whether the flexibility of the module is considered. Wu et al. (1993) evaluated the hydroelastic response of a modular floating island composed of five semi-submersible modules by applying a flexible module and flexible connector model. Zhang et al. (2015) analyzed motion response by applying a rigid module and flexible connector model to a marine airport composed of multiple pontoon type modules. In order to apply the rigid module and flexible connector model, the hydrodynamic coefficients were derived using a linear wave theory and an eigen-function expansion method. Riggs et al. (2000) calculated a similar motion response and connector force using a rigid module and flexible connector model as well as a flexible module and flexible connector model for a modular floating island composed of 300 m long modules. This demonstrated that the motion response of a modular floating island can be evaluated based on a rigid module and flexible connector model, which is a relatively simple model. Otto et al. (2019a) analyzed motion response by applying the modular floating island proposed by the Space@Sea project as a rigid module and flexible connector model. Waals et al. (2018) verified the validity of the analysis

technology through comparison with the model test results.

In this study, the wave-induced motion response of a floating island composed of a number of pontoon-type modules was analyzed based on a potential flow-based numerical analysis method in the frequency domain. In Section 2, a numerical method was presented to evaluate the motion response of a modular floating island. The modular floating island was modeled with a number of rigid modules and flexible connectors by applying potential flow-based hydrodynamic coefficients. In Section 3, the validity of the present numerical method was examined by comparing it with the existing model test results of a modular floating island (Waals et al., 2018). In Section 4, the configuration of the modular floating island is divided into 'central modules', 'tail module', and 'outer modules'. Then the effects of the arrangement and size of each module on the motion characteristics of floating islands in waves were discussed.

2. Numerical Analysis Method

2.1 Higher-order Boundary Element Method

This study applied a potential flow model to analyze the motion response of floating bodies in waves. In the potential flow theory where inviscid, incompressible fluid and irrotational flow are assumed, the boundary value problem for linear velocity potential is formulated as Eqs. (1) to (5).

$$\nabla^2 \phi = 0 \quad \in \Omega \tag{1}$$

$$\frac{\partial \phi}{\partial t} + g\zeta = 0, \quad \frac{\partial \zeta}{\partial t} - \frac{\partial \phi}{\partial z} = 0 \quad on \ z = 0 \tag{2}$$

$$\frac{\partial \phi}{\partial n} = v_n \quad on \ S_B \tag{3}$$

$$\frac{\partial \phi}{\partial n} = 0 \quad on \ S_W \tag{4}$$

$$\lim_{kr \to \infty} \sqrt{kr} \left(\frac{\partial \phi_j}{\partial r} - k\phi_j \right) = 0 \tag{5}$$

Here, Ω denotes the entire fluid domain. S_B and S_W represent the boundaries of the floating body surface and the sea bottom, respectively. ϕ is the linear velocity potential for the flow. g denotes the gravitational acceleration, and ζ denotes the wave height. n and v_n are the normal vector and normal velocity defined on the floating body surface or the sea bottom, respectively. z denotes the coordinate in the vertical direction with respect to the free surface. k and r are the wave number and the diameter of the boundary, respectively. Eq. (1) is the Laplace equation, which is the governing equation for the fluid domain based on the potential flow theory. Eq. (2) indicates the dynamical and kinematic boundary conditions on the free surface, respectively. Eqs. (3) and (4) are the non-penetration boundary conditions for the floating body surface and sea bottom, respectively. Eq. (5) corresponds to the

radiation condition at the far field.

To solve the linear boundary value problem described above, the higher-order boundary element method was applied in this study. To this end, the floating body surface was discretized with 9-node biquadratic elements. Numerical solutions with the higher-order boundary element method have been found to have higher accuracy and convergency than the constant panel method (Choi and Hong, 2002). It has also been extensively applied to the problem of multiple floating bodies with complex shapes (Nam and Hong, 2021). The following equation represents the integral equation for the boundary value problem using the wave Green function:

$$\phi(\vec{r_0})[1+\nu\iint_{S_B} G(\vec{r},\vec{r_0})dS] + \iint_{S_B}[\phi(\vec{r})-\phi(\vec{r_0})]G(\vec{r},\vec{r_0})dS$$
$$= \iint_{S_B}\phi_n(\vec{r})G(\vec{r},\vec{r_0})dS \quad (6)$$

where $\vec{r_0}$ denotes the coordinates of the source point distributed on the panel.

Complex flows occur in the narrow gap space between the modules of a modular floating island. Strong vortex is generated at the edge of the module, and the viscous drag becomes significant. To consider the damping effect of this flow, the modified body boundary condition in E. (7) was applied to reflect the viscous damping effect, which is similar to the method applied to the sloshing flow problem by Zalar et al. (2007).

$$\frac{\partial\phi}{\partial n} = i\epsilon k_0\phi + v_n \quad on\ S_B \quad (7)$$

where $k_0 (=\omega^2/g)$ is the wave number at infinite depth and ω is the wave frequency. ϵ is a parameter that controls the degree of numerical damping. In this study, 0.02 was applied for ϵ.

2.2 Evaluation of Stiffness Matrix

With regard to mooring and connector problems between multiple floating bodies, a linear stiffness matrix can be derived considering the pretension and spring stiffness components (Nam and Hong, 2021). The first stiffness component is proportional to the pretension and the change in the angle of the mooring line, while the second stiffness component is proportional to the change in the length of the mooring line. In this study, complex connectors between modules of the floating island were simplified with equivalent springs, and the motion of the floating island was analyzed in consideration of the linear stiffness matrix by the equivalent springs. To derive the global stiffness matrix of the floating island, the local stiffness matrix is first derived according to the connectors' positions between unit modules, and then it is converted into a global stiffness matrix by applying a conversion matrix. Subsequently, the same process is repeated for all connectors to finally obtain the total global stiffness matrix of the modular floating island.

First, a stiffness component for the connector between the modules J_1 and J_2 can be represented as a local stiffness matrix ($[K^e]_{3\times6}$) as follows:

$$\begin{Bmatrix}F_{n+1}\\F_{n+2}\\F_{n+3}\end{Bmatrix} = [K^e]_{3\times6}\begin{Bmatrix}s_{n+1}\\s_{n+2}\\s_{n+3}\\s_{n+4}\\s_{n+5}\\s_{n+6}\end{Bmatrix}, \quad [K^e]_{3\times6}=\begin{bmatrix}-k_x & 0 & 0 & k_x & 0 & 0\\0 & -k_y & 0 & 0 & k_y & 0\\0 & 0 & -k_z & 0 & 0 & k_z\end{bmatrix} \quad (8)$$

where F_{n+1}, F_{n+2}, and F_{n+3} are the restoring forces acting on the module J_1, while F_{m+1}, F_{m+2}, and F_{m+3} are the restoring forces acting on the module J_2. $n=6\times(J_1-1)$ and $m=6\times(J_2-1)$ are integers for the degree of freedom of the two modules, respectively. s_n is the local motion of nth degree of freedom at the connector position, and (k_x,k_y,k_z) are the components of the spring stiffness. Then, the local stiffness matrix can be converted into a global stiffness matrix using a transformation matrix ($[T^e]_{6\times12}$) as follows:

$$\begin{Bmatrix}s_{n+1}\\s_{n+2}\\s_{n+3}\\s_{n+4}\\s_{n+5}\\s_{n+6}\end{Bmatrix} = [T^e]_{6\times12}\begin{Bmatrix}\xi_{n+1}\\\xi_{n+2}\\\xi_{n+3}\\\xi_{n+4}\\\xi_{n+5}\\\xi_{n+6}\\\xi_{m+1}\\\xi_{m+2}\\\xi_{m+3}\\\xi_{m+4}\\\xi_{m+5}\\\xi_{m+6}\end{Bmatrix}, \quad [T^e]_{6\times12}=\begin{bmatrix}1&0&0&0&z_1&-y_1&0&0&0&0&0&0\\0&1&0&-z_1&0&x_1&0&0&0&0&0&0\\0&0&1&y_1&-x_1&0&0&0&0&0&0&0\\0&0&0&0&0&0&1&0&0&0&z_2&-y_2\\0&0&0&0&0&0&0&1&0&-z_2&0&x_2\\0&0&0&0&0&0&0&0&1&y_2&-x_2&0\end{bmatrix}$$
$$(9)$$

where (x_1,y_1,z_1) and (x_2,y_2,z_2) correspond to the positions where the connectors of modules J_1 and J_2 are attached. Considering the rotation matrix ($[R^e]_{3\times3}$) for the moment of rotational motion, the stiffness matrix ($[K]$) by the connector can be calculated as follows:

$$\begin{Bmatrix}F_{n+1}\\F_{n+2}\\F_{n+3}\\F_{n+4}\\F_{n+5}\\F_{n+6}\\F_{m+1}\\F_{m+2}\\F_{m+3}\\F_{m+4}\\F_{m+5}\\F_{m+6}\end{Bmatrix} = \begin{bmatrix}[K^e]_{3\times6}[T^e]_{6\times12}\\[R^e]_{3\times3}[K^e]_{3\times6}[T^e]_{6\times12}\\-[K^e]_{3\times6}[T^e]_{6\times12}\\-[R^e]_{3\times3}[K^e]_{3\times6}[T^e]_{6\times12}\end{bmatrix}\begin{Bmatrix}\xi_{n+1}\\\xi_{n+2}\\\xi_{n+3}\\\xi_{n+4}\\\xi_{n+5}\\\xi_{n+6}\\\xi_{m+1}\\\xi_{m+2}\\\xi_{m+3}\\\xi_{m+4}\\\xi_{m+5}\\\xi_{m+6}\end{Bmatrix} = [K]\begin{Bmatrix}\xi_{n+1}\\\xi_{n+2}\\\xi_{n+3}\\\xi_{n+4}\\\xi_{n+5}\\\xi_{n+6}\\\xi_{m+1}\\\xi_{m+2}\\\xi_{m+3}\\\xi_{m+4}\\\xi_{m+5}\\\xi_{m+6}\end{Bmatrix}$$

where, $[R^e]_{3\times3}=\begin{bmatrix}0 & -z_1 & y_1\\z_1 & 0 & -x_1\\-y_1 & x_1 & 0\end{bmatrix}$ \quad (10)

3. Validation of Numerical Method

3.1 Module Specifications

To validate the numerical method of this study, the present calculation results are directly compared with the model test data on modular floating islands by Waals et al. (2018). A model test was conducted for a floating island made of modules in the shape of an equilateral triangular prism of two sizes (Fig. 1) at MARIN (Maritime Research Institute Netherlands) by Waals et al. (2018). In this study, this modular floating island concept is referred to as the 'MARIN model'. The principle dimensions of the triangle modules by Waals et al.(2018) are shown in Table 1. Here, the dimensions are based on the real-scale values which are obtained by converting the model test dimensions by considering the model test scale ratio (1:250). As shown in Table 1, the dimensions of a small triangle module with a length of 237 m are listed in the first column, and the dimensions of a large triangle module with a length of 487 m are listed in the second column. Here, the distance between the triangle modules was assumed as 7.5 m, which is the length in which the four little triangle modules has the same size as the giant triangle module. This is approximately 2% more than the 7.35 m by Waals et al. (2018). The same radius of gyration as Waals et al. (2018) was used for present numerical analysis, which corresponds to about 68% of the radius of gyration in the case of a uniform mass distribution. In this study, a hexagon module was newly introduced to check the effect of the central module arrangements. In this case, the length parameters of the hexagon modules were determined to match the combined form of six big triangle modules. By extending the radius of gyration of the triangle modules, the radius of gyration of hexagon modules was calculated, which also corresponds to 68% of the radius of gyration of hexagon modules with a homogeneous mass distribution. The center of gravity in the vertical direction of the triangle and hexagon modules was assumed as the same as the still water level. The shape and panel distribution of the modules are depicted in Fig. 2. Because the floating island should be represented by a number of modules, it is necessary to determine the number of panels per module considering not only the accuracy of the solution but also the efficiency of the calculation. The grid convergence for triangle modules was analyzed in this work, and the number of panels (elements) was determined to have an inaccuracy of less than 0.5% based on motion response. Triangle modules were discretized with 45 higher-order elements in total, and the hexagonal module was represented by 198 elements. In the vertical direction, a single higher order element was applied to both triangle modules and hexagon modules.
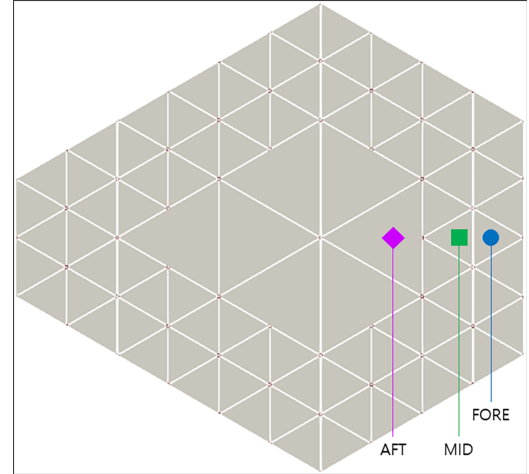

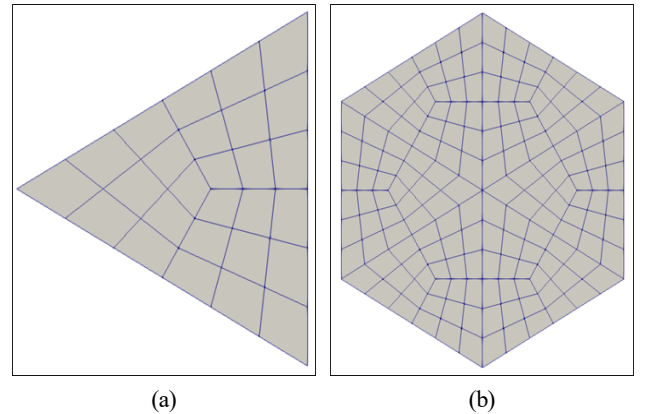**Fig. 1** Module arrangements of MARIN model (Waals et al, 2018)

| (a) | (b) |

Fig. 2 Panel distributions of triangle and hexagon module: (a) Triangle module; (b) Hexagon module.

Table 1 Principal dimensions of the floating structure modules

Item	Small triangle	Large triangle	Hexagon
Displacement (m³)	2.171×10^5	9.166×10^5	5.697×10^6
Length (m)	237	487	495.66
Longitudinal length (m)	$L_{x,small} = 205.25$	$L_{x,large} = 421.75$	$L_{x,hexagon} = 858.51$
Draft (m)	8.925	8.925	8.925
$Kxx^{1)}$ (m)	27.3	67.54	153.71
$Kyy^{2)}$ (m)	32.6	67.54	153.71
$Kzz^{3)}$ (m)	40.9	94.85	217.38

[1)] Radius of gyration about x axis
[2)] Radius of gyration about y axis
[3)] Radius of gyration about z axis

3.2 Connectors Between Modules

Waals et al. (2018) used fenders and springs to represent connectors between unit modules of the floating artificial island in their model test. The fender provides elastic force only when compressed, generating a supporting force that keeps the spacing between modules from narrowing. The spring, on the other hand, provides a force proportional to displacement equally during compression and relaxation, which generates a restoring force to maintain the separation distance between modules. During the model test, it was confirmed that the fender remained in contact with the module due to the initial tension of the springs. In this case, the fender was inserted to receive force perpendicular to the module's side, and a number of springs were installed at an angle of 45 degrees on the facing surface of the adjacent module. Thus, an equivalent spring corresponding to the fender and the springs was introduced to link the modules in this numerical analysis, and the stiffness of the spring used in the analysis was 187,250 kN/m. In addition, although the spring and fender are utilized for the horizontal connection, vertical frictional force may arise owing to the compressed fender. As a result, even for vertical motion, the restoring force must be considered. Otto et al. (2019b) conducted a numerical study by modeling the vertical shear force induced by the connector with a force proportionate to vertical deformation. In this study, a vertical spring with a stiffness of 87,500 kN/m, which corresponds to about 47% of the stiffness on the horizontal plane, was used in the numerical analysis.

3.3 Validation

To validate the present numerical method, the calculated heave and pitch motion RAOs (response amplitude operator) of the unit floating modules were directly compared with the measured experimental data of the model test. The representative positions for the motion responses of three floating modules were labeled as 'AFT', 'MID', and 'FORE', and each position is remarked in Fig. 1. Fig. 3 shows the comparison results of the heave and pitch motion RAOs of three

floating modules. The numerical analysis results are denoted by lines, whereas the model test results are represented by symbols. The numerical results are based on the frequency-domain analysis, where the motion RAO values are calculated individually for each frequency. In the case of the model test, the motion RAOs of the modules were estimated by using the motion response spectra and wave spectrum measured from the irregular wave test. The numerical and experimental data show a slight difference in motion RAOs around a wave frequency of 0.5 rad/s, but overall motion responses show a similar tendency. The heave motion RAO of the FORE and MID modules is approximately 1.5 around the wave frequency of 0.3 rad/s ($\lambda/L_{x,small} = 3.34$), whereas the AFT module showed a smaller heave RAO than the other modules at all frequencies. The small motion response of the AFT module can be interpreted as an insignificant wave excitation effect due to its relatively large size and location away from the outside. In higher frequencies than 0.3 rad/s, both numerical and experimental results showed a decreasing tendency of the heave and pitch RAOs as the wave frequency increased. Looking at the module's pitch RAO, the closer the module is to the incident wave direction, the larger the peak response occurs at a higher wave frequency. From the results of Fig. 3, it can be confirmed that, even though the FORE module and MID module are the same size, the magnitude of the response and the peak period differ based on the location and connection method.

4. Results and Discussions

According to the planar arrangement of the modules, the modular floating island can be divided into three parts, as illustrated in Fig. 4. The "central modules" are the large triangle modules that make up the central section. The term "tail module" was used to describe the large triangle module that is located behind the central modules, while the word "outer modules" was used to describe the outermost modules that surround the tail module and the central modules. In this study,
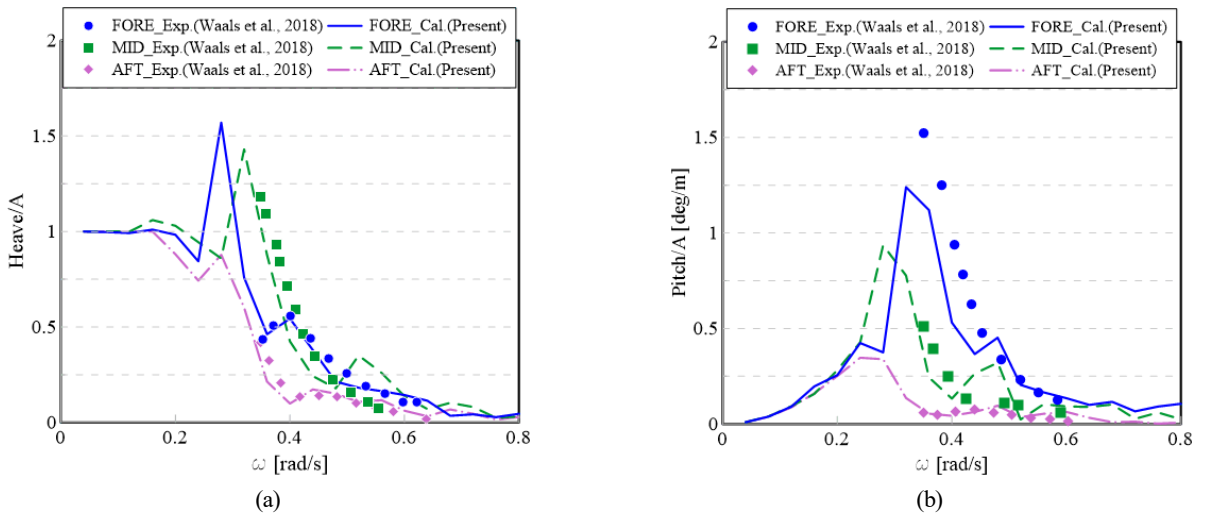

(a)

(b)

Fig. 3 Comparison of motion RAOs of the modules (FORE, MID and AFT) between the experimental model and present numerical model: (a) Heave motion; (b) Pitch motion.
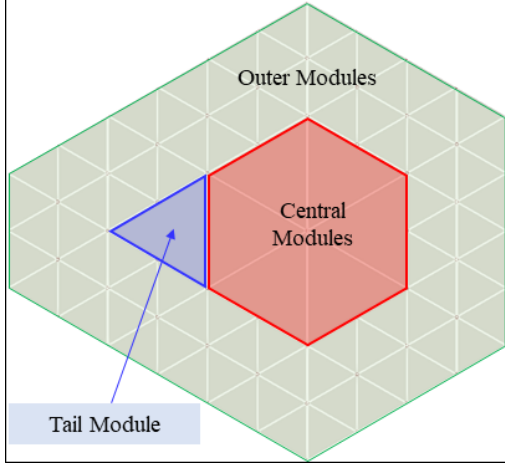
Fig. 4 Definition of module sections of floating island model

the effect of module size and arrangement on the motion performance of the floating island was examined. All numerical analyses made use of the assumption of deep water and head wave, which corresponds to the case where the incident wave propagates from the right to the left in Fig. 4.

4.1 Effect of Tail Module

The motion responses were compared between the original MARIN model and the newly proposed "Floater A" model in order to examine the effects of the tail module, as shown in Fig. 5. In the case of the Floater A model, the arrangement of the outer modules becomes symmetrical by removing the tail module. Focusing on the motion response of the modules on the weather side, a comparison was conducted between the 'HEAD' module at the outermost edge (square/rhombus symbol in Fig. 5) and the 'MID' module at the inside (circle/triangle symbol in Fig. 5). Fig. 6 compares the heave and pitch RAOs of the two outer modules between the MARIN model (solid line) and Floater A (dotted line). At $\omega = 0.2\,rad/s$, there is a slight difference in heave RAO due to the tail module, but overall, it can be seen that the effect of tail module on the motion RAOs of the outer modules is not significant. This indicates that the interaction effect is not strong owing to the large separation distance between the tail module and the front outer modules, and the effect of tail module on the overall motion response characteristics of the floating island is quite small. When comparing the motion response characteristics of the two outer modules at frequencies higher than 0.36 rad/s, the HEAD
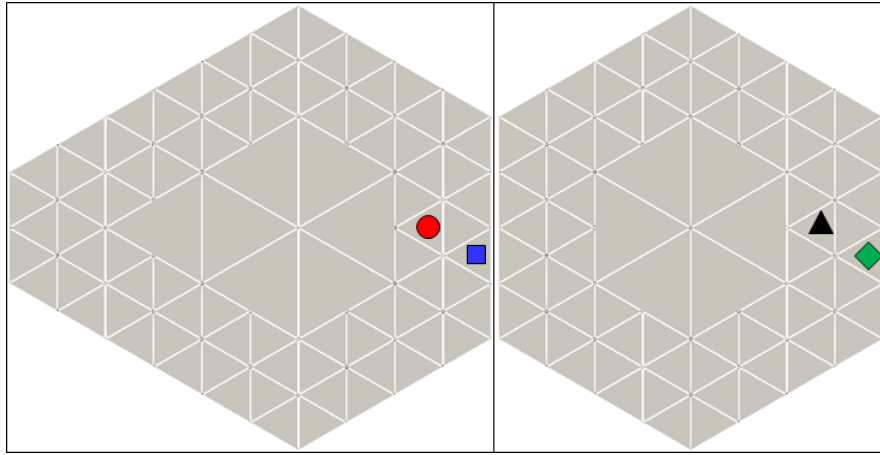

Fig. 5 Module arrangement of floating island models with and without tail module (left: MARIN model, right: Floater A)
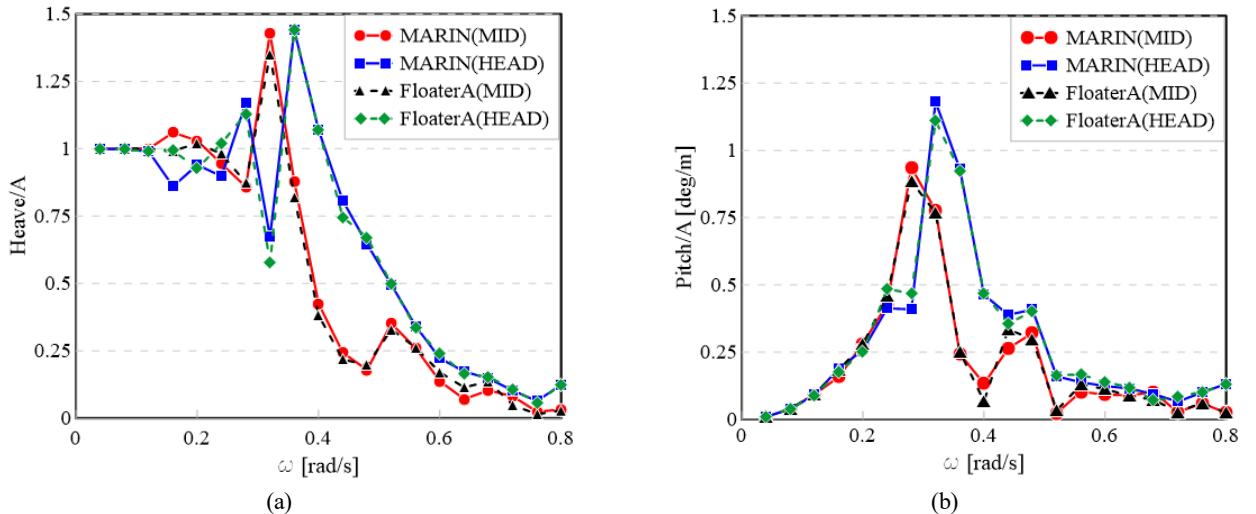

(a)   (b)

Fig. 6 Comparison of motion RAOs between floating island models with and without tail module: (a) Heave motion; (b) Pitch motion.

(a)   (b)   (c)
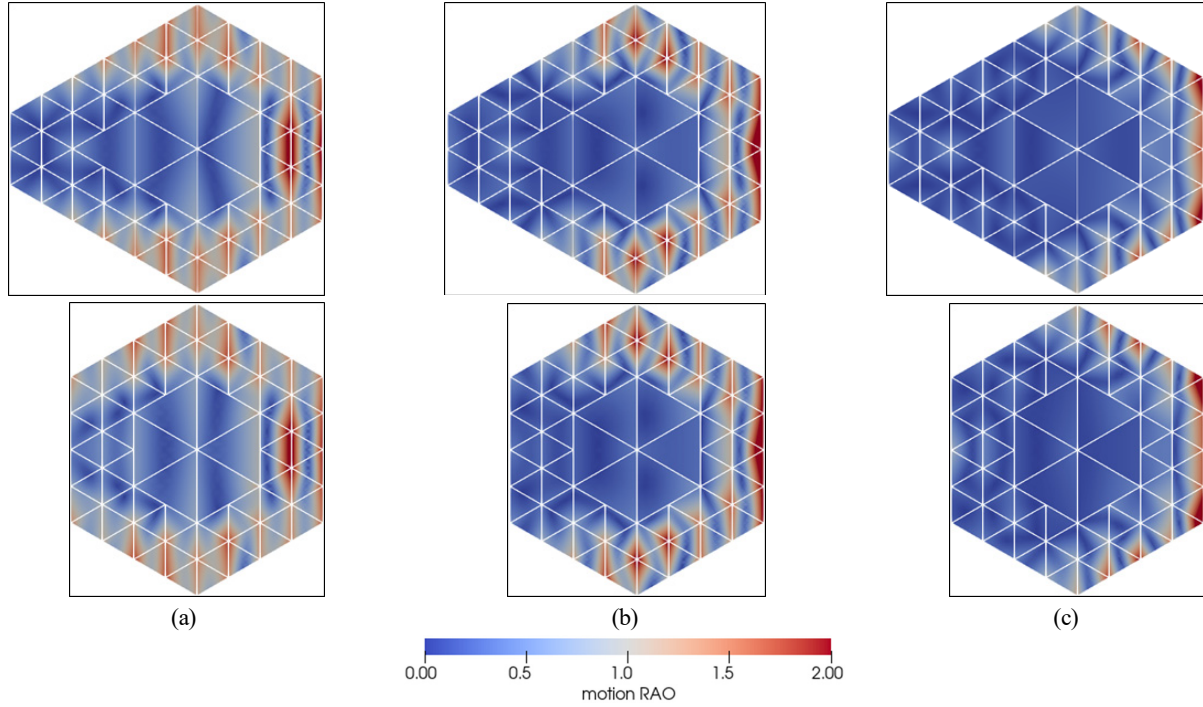
Fig. 7 Comparison of contour plots of vertical motion responses between floating island models with and without tail module: (a) ω = 0.32 rad/s; (b) ω = 0.36 rad/s; (c) ω = 0.4 rad/s

module consistently showed larger heave and pitch motions than the MID module. This means that when a high-frequency short wave is incident, only the outermost modules on the weather side are mainly excited, and the motions of the modules positioned farther within are reduced. In this case, most of the incident waves are reflected, creating high waves in front of the outer modules.

In the frequency range of 0.28 to 0.4 rad/s, the HEAD and MID modules exhibit large heave and pitch motion responses. The contour plots in Fig. 7 compares overall vertical motion response distribution of the two floating islands at three frequency conditions (ω = 0.32, 0.36, and 0.40 rad/s). First, both floating island models show that the vertical motion of the central modules is relatively less than that of the adjacent outer modules. This is because the outer modules move by absorbing the wave energy, and the wave exciting forces acting on the central module are significantly reduced. Another reason is that the central module has about 4 times inertia of the outer module. Another pattern in the contour plots is that the vertical motion increases intensively in the outer modules on the weather side (right side of the figure) under the short wave conditions and rapidly decreases on the opposite side. This is consistent with the numerical analysis results of Otto et al. (2019a), which show that at the peak frequency where the maximum motion of the modular floating island occurs, the modules on the lee side exhibit a very small motion, while the modules on the weather side experience a large motion. This feature indicates that the modules on the weather side absorb the majority of the wave kinetic energy under the short wave conditions, which leads to reduced motion responses of the other modules. When comparing the motion responses of two floating islands at the three frequencies, the MARIN model and Floater A show very similar patterns of vertical motion

response distribution. This indicates that there is only a small effect of the tail module on the vertical motion of the floating island since it is placed in the opposite direction of the incident wave.

4.2 Effect of Central Modules

The advantage of a modular floating island is that the motion responses of the central modules and the lee-side modules are greatly reduced since the modules on the weather side absorb a large portion of the wave kinetic energy. Due to these characteristics, the central module exhibit a small motion response even if waves approach from various directions. The placement of large facilities like residential structures and essential equipment is therefore possible in the central modules of modular floating islands. In this section, a numerical analysis was conducted to examine the effect of the central module on the motion response of floating island. Fig. 8 illustrates the plan views of the "Floater A" and "Floater B" models depending on whether the
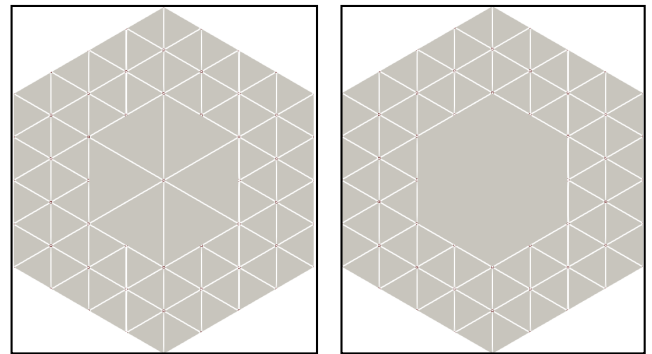

Fig. 8 Module arrangements of floating island model with different central modules (left: Floater A, right: Floater B)

central module of the floating island is divided. The central modules of "Floater A" are composed of six triangle modules, but the central module of "Floater B" is made up of one hexagon module.

Fig. 9 shows the comparison results of the heave and pitch RAOs for the central modules of Floaters A and B. In the case of Floater A, since the central part is made up of six modules, the motion response of the central modules was evaluated by the average of the motion responses of the triangle modules. The central module of Floater B shows smaller heave and pitch responses than that of Floater A in all frequency ranges. It can be seen that the motion performance of the single central module is better than that of divided central modules under all wavelength conditions. In Fig. 9(b), the central modules of Floater A have the maximum pitch response at a wave frequency of about 0.25

rad/s, in which the half of the incident wavelength (493 m) at this frequency is similar to the transverse length of the triangle modules ($\lambda/2L_{x,large} = 1.17$). Floater B shows the maximum pitch RAO at the wave frequency of 0.2 rad/s. Here, the length ratio between the transverse length of the central hexagon module and the half of the incident wavelength is approximately 0.9 ($\lambda/2L_{x,hexagon} = 0.9$). This indicates that the peak period of pitch motion can change depending on whether the central module is divided, and the pitch RAO of the central module has the maximum value under the condition that the wavelength of the incident wave corresponds to about twice the length of the central module. In this section, it was found that when using a single central module, not only heave and pitch motions are reduced, but also the peak frequency of pitch motion shifts to a lower frequency
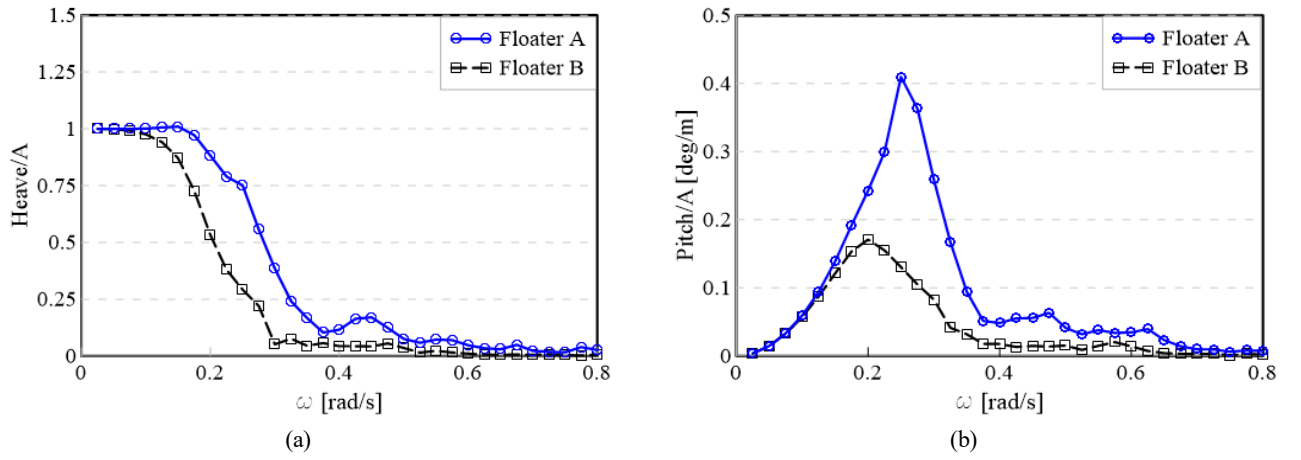

Fig. 9 Comparison of motion RAOs central modules between the Floater A and B models: (a) Heave motion; (b) Pitch motion
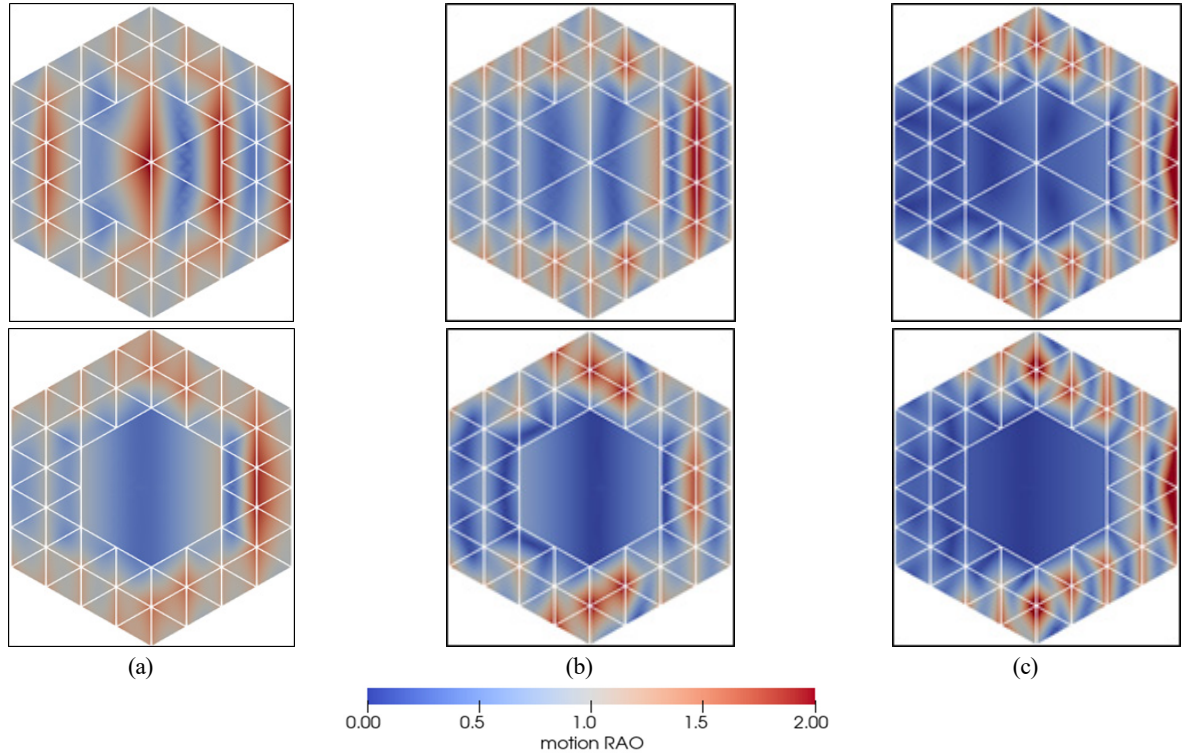

Fig. 10 Comparison of contour plots of vertical motion responses between floating island models with different central modules: (a) ω = 0.25 rad/s; (b) ω = 0.3 rad/s; (c) ω = 0.35 rad/s

than when using divided central modules. Therefore, a large single central module may be a good design alternative to reduce the wave-induced motion of modular floating island.

To check the effect of the central modules on the overall vertical motion of the floating island, the motion response of the entire floating island was visualized in the frequency range of $\omega = 0.2 - 0.3$ rad/s, where the central modules show a relatively large motion response. Fig. 10 shows contour graphs of the vertical plane motion amplitude distribution for the floating island for the three frequency conditions of $\omega = 0.25, 0.30,$ and 0.35 rad/s. First, the central module of Floater B clearly shows a smaller vertical motion than the central modules of Floater A regardless of the wave frequencies. This means that the single central module reduces the local vertical motion responses compared to the divided central modules. Additionally, as discussed in the previous section, as the wave frequency increases, it can be also confirmed that vertical motion is concentrated on the outer module facing the incoming wave. On the other hand, it is remarkable that the vertical motion distribution characteristics of the outer modules differ significantly depending on whether or not the central modules are divided. This is because the vertical force of the connector between the central modules and the outer modules is affected by the motion performance of the central modules, and the mechanical interactions via these connectors significantly changes the motion characteristics of the outer modules. This effect is observed in the outer modules located on the front and side of the central modules.

4.3 Effect of Outer Modules

The outer module absorbs the wave kinetic energy and contributes to the motion reduction of the central module. Therefore, it is necessary to investigate the effect of the arrangement and configuration of the outer module layer on the motion reduction of the central module. In this section, 'Floater C' model was introduced by changing the size of the outer modules, and the effect of the number of outer module layers on
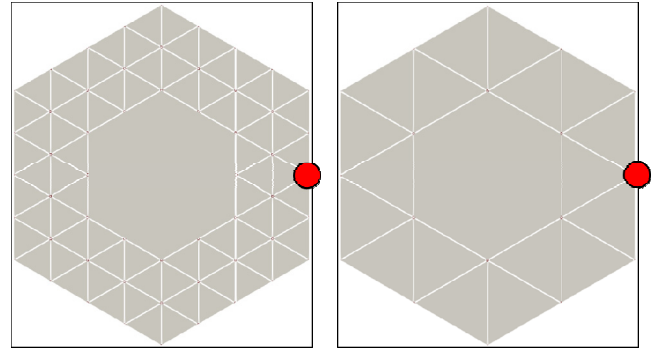

Fig. 11 Module arrangements with single-layer and double-layers outer modules (left: Floater B, right: Floater C)
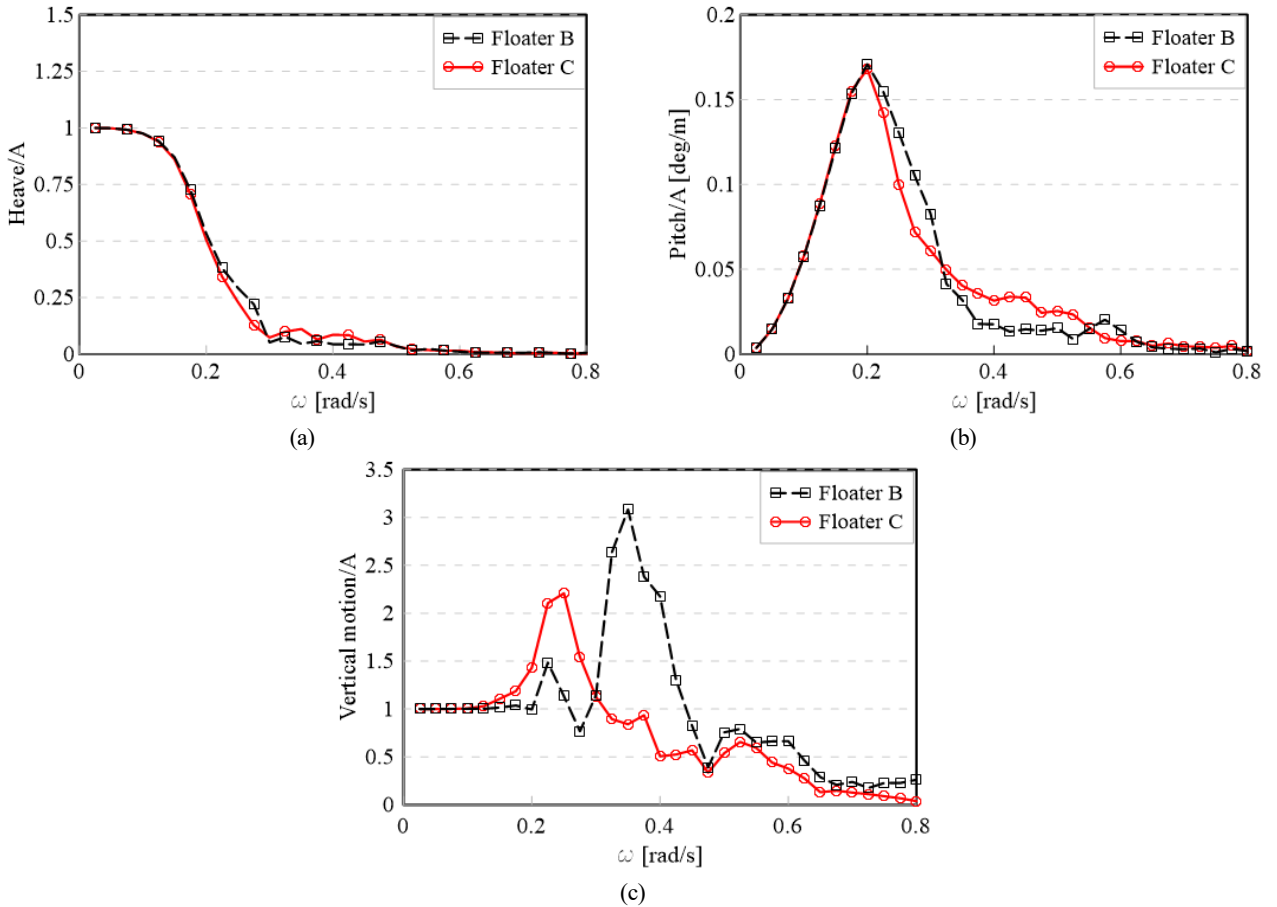

(a)

(b)

(c)

Fig. 12 Comparison of motion RAOs of central modules between floating island models with the single outer layer (Floater C) and double outer layer (Floater B): (a) Heave motion (central module); (b) Pitch motion (central module); (c) Vertical motion (outer module)

the motion response of the floating island was examined. Fig. 11 shows the plan view of the floating island models with single-layer (Floater C) and double-layers (Floater B) of outer modules.

Fig. 12 compares the heave and pitch RAOs between Floater B and Floater C. As shown in the figure, the effect of the outer layer on the central module was insignificant under the long waves in the frequency lower than 0.2 rad/s. However, Floater B and Floater C show a noticeable difference in the motion RAOs of the central module in the frequency higher than 0.2 rad/s. In particular, the motion RAOs of the central modules of both floating islands showed an opposite frequency dependence based on the wave frequency of 0.3 rad/s ($\lambda/L_{x,small}$ = 3.34). In other words, Floater C showed smaller heave and pitch response than Floater B at frequencies lower than 0.3 rad/s, whereas the opposite pattern was seen at frequencies higher than 0.3 rad/s. To examine the detailed motion characteristics, Fig. 12(c) compares the local vertical motion RAO of the outer modules of Floater B and Floater C. Since the motion response of the outer modules varies depending on the position of the module, the local vertical motion was examined for the outer end position of the outer modules (red dot position in Fig. 11), which exhibits a large vertical motion by directly facing the wave. The vertical motion response of the outer modules likewise altered at a frequency of 0.3 rad/s and shows the opposite tendency to the motion of the central modules. At

frequencies below 0.3 rad/s and above 0.3 rad/s, the local vertical motion of the outer modules of Floaters B and C was smaller, respectively.

As mentioned above, the central and outer modules of Floater B and Floater C show different motion characteristics depending on the frequency. The motion responses of the floating island in irregular waves were assessed in order to compare the motion performance in real sea states. Based on the Pierson-Moskowitz (PM) spectrum, the significant wave height (H_s) of the irregular wave was set at 11.5 m, and the peak period (T_p) was changed to 14.5 s, 16.0 s, 17.5 s, and 19.0 s.
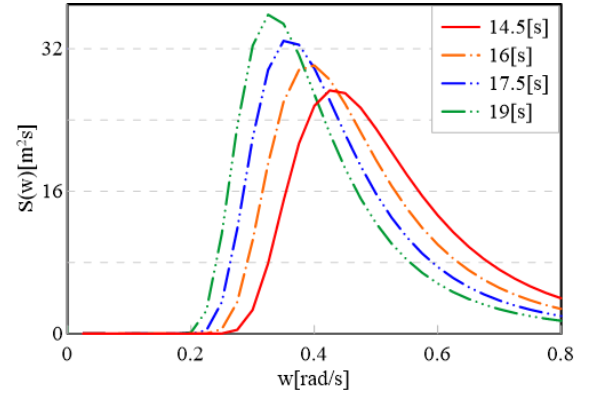

Fig. 13 Wave spectra for 4 irregular wave conditions
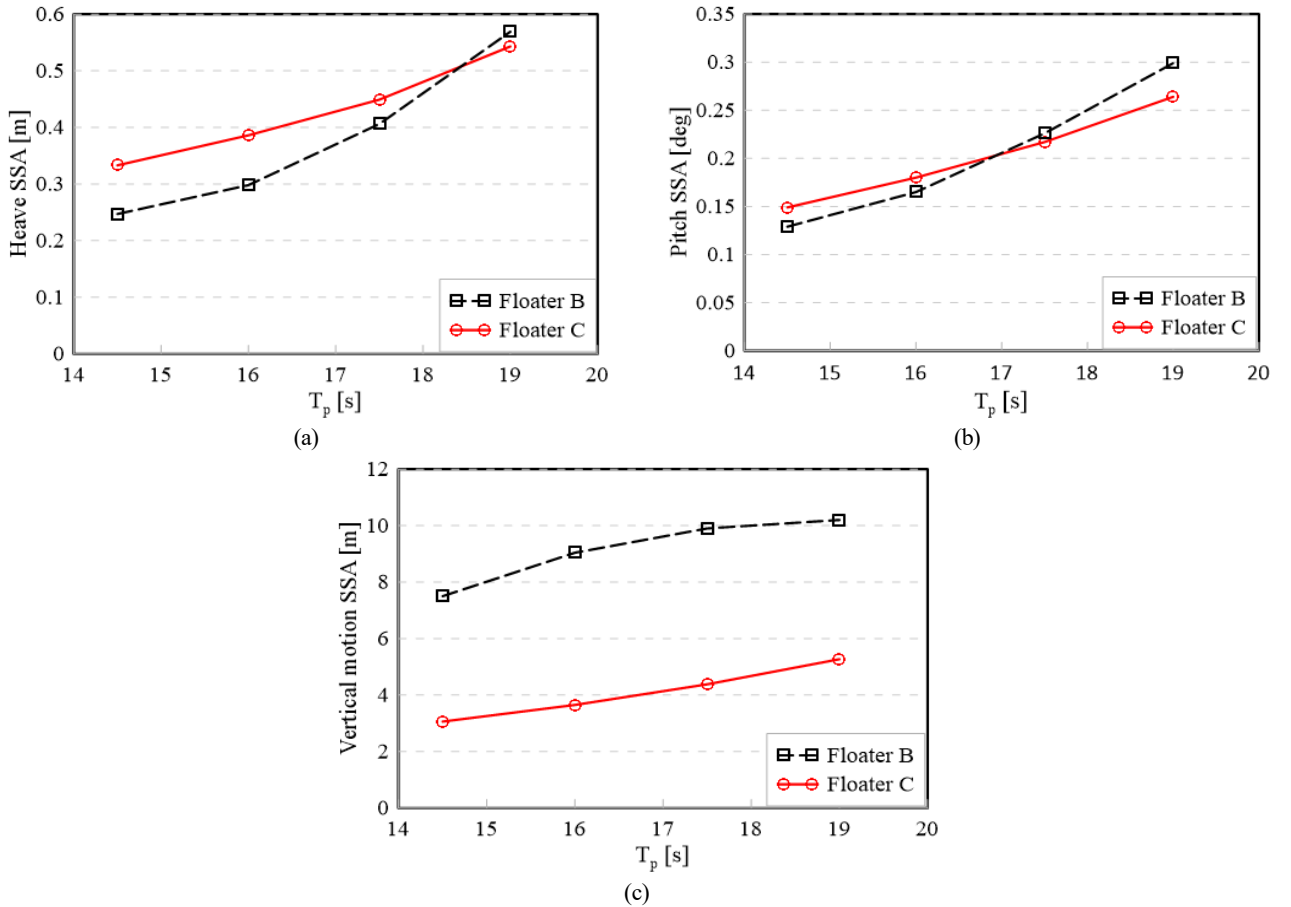

(a)

(b)

(c)

Fig. 14 Comparison of single significant response of heave and pitch motion of Floater B and C in irregular waves: (a) Heave motion (central module); (b) Pitch motion (central module); (c) Vertical motion (outer module)

This allowed for the consideration of a total of four irregular wave conditions. Fig. 13 shows the four irregular wave spectra considered in the motion performance evaluation of this study.

The motion responses of the floating island in irregular waves were calculated based on the frequency-domain spectral method by applying the following equations:

$$S_j(w) = \left| \overline{\eta_j}(w) \right|^2 S_\zeta(w) \tag{11}$$

$$\xi_j = 2 \sqrt{\int S_j(w) dw} \tag{12}$$

where S_ζ and S_j are the response spectra of the wave spectrum and the jth motion mode of the floating island, respectively. Furthermore, $\overline{\eta_j}$ denotes the transfer function of the floating island's jth motion mode, and ξ_j denotes the single significant response for the jth motion mode.

The heave and pitch responses of central modules under four irregular wave conditions are compared in Fig. 14(a) and (b). A comparison of the local vertical motion response at the ends of the outer modules is shown in Fig. 14(c). In the case of the central modules, Floater B had a higher sensitivity of motion response according to the change of peak frequency than Floater C. The heave and pitch responses of Floater B increased by about 2.3 times and 2.32 times as the peak period of irregular wave changes from 14.5 s to 19.0 s, respectively. Under the same conditions, the heave and pitch responses of Floater C increased by about 1.63 and 1.77 times, respectively. As a result, the central modules of Floater B showed better motion performance in the sea states with a relatively short period. On the other hand, the motion response of the central modules of Floater C became smaller than that of Floater B under the peak period condition of 18.0 s or longer. This indicates that the double-layer outer part with small unit modules is more effective in calming the central modules than the single-layer outer part, except for the long period condition of 18.0 s or longer. In the case of the outer modules, it can be seen that the vertical motion of Floater C is around 2 to 2.5 times smaller than that of Floater B under the given irregular wave condition. This shows that Floater B, which employs small unit modules in the outer part, absorbs the wave kinetic energy better than Floater C, which employs large outer modules, and the outer modules of Floater B exhibit larger vertical motion responses.

5. Conclusions

The motion response of a modular floating island was numerically analyzed in this study. A potential flow-based numerical analysis method for the modular floating island was proposed. Numerical validation was performed by directly comparing the present calculation results with the model test data for the modular floating island by Waals et al. (2018). In this study, the modular floating island was divided into three parts; a tail module, central modules, and outer modules. The vertical motion responses was examined according to

the module size and arrangement by a series of numerical studies. First, the effect of the tail module on the vertical motion was insignificant, whereas the change in the motion response of the floating island was clearly observed depending on the division effect of the central module. It was confirmed that the vertical motion of the central module was reduced and the peak period shifted to a lower frequency range when a single central module was used than divided small central modules. Next, depending to the size of the outer modules and the number of outer layers, the change in heave and pitch of the central modules was negligible in the low frequency region, but significant in the high frequency region. In particular, through irregular wave analysis, the double-layer outer part with small unit modules is more effective in calming the central modules than the single-layer outer part with large unit modules, except under very long period conditions. It was observed that the wave kinetic energy is better absorbed when a small unit module is employed on the outer part. Future research must look more closely at the motion characteristics of the floating island with moorings in the horizontal plane, and the optimization of the unit module shape and connector for the modular artificial floating island.

Conflict of Interest

No potential conflict of interest relevant to this article was reported.

Funding

References

Yeh, N., Yeh, P., & Chang, Y. -H. (2015). Aritificial floating islands for environmental improvement. *Renewable and Sustainable Energy Reveic, 47*, 616−622. https://doi.org/10.1016/j.rser.2015.03.090

Lu, H. -L., Ku, C. -R., & Chang, Y. -H. (2015). Water quality improvement with artificial floating islands. *Ecological Engineering, 74*, 371−375. https://doi.org/10.1016/j.ecoleng.2014.11.013

Wang, C. M. & Tay, Z. Y. (2011). Very large floating structures: applications, research and development. *Procedia Engineering, 14*, 62−72. https://doi.org/10.1016/j.proeng.2011.07.007

Lamas-Pardo, M., Iglesias, G., & Carral, L. (2015). A review of very

large floating structures (VLFS) for coastal and offshore uses. *Ocean Engineering, 109*, 677−690. https://doi.org/10.1016/j.oceaneng.2015.09.012

Kashiwagi, M. (1998). A B-spline Galerkin scheme for calculating the hydroelastic response of a very large floating structure in waves. *Journal of Marine Science and Technology, 3*, 37−49. https://doi.org/10.1007/BF01239805

Watanabe, E., Utsunomiya, T., & Wang, C.M. (2004). Hydroelastic analysis of pontoon-type VLFS: a literature survey. *Engineering Structures, 26*(2), 245−256. https://doi.org/10.1016/j.engstruct.2003.10.001

Wu, Y., Wang, D., Riggs, H. R., & Ertekin, R. C. (1993). Composite singularity distribution method with application to hydroelasticity. *Marine Structures, 6*(2-3), 143−163. https://doi.org/10.1016/0951-8339(93)90017-W

Riggs, H. R., Ertekin, R. C., & Mills, T. R. J. (2000). A comparative study of RMFC and FEA models for the wave-induced response of a MOB. *Marine structures, 13*(4-5), 217−232. https://doi.org/10.1016/S0951-8339(00)00029-0

Fu, S., Moan, T., Chen, X., & Cui, W. (2007). Hydroelastic analysis of flexible floating interconnected structures. *Ocean engineering, 34*(11-12), 1516−1531. https://doi.org/10.1016/j.oceaneng.2007.01.003

Kim, J. -G., Cho, S. -P., Kim, K. T., & Lee, P. -S. (2014). Hydroelastic design contour for the preliminary design of very large floating structures. *Ocean Engineering, 78*, 112−123. https://doi.org/10.1016/j.oceaneng.2013.11.006

Gao, R. P., Tay, Z. Y., Wang, C. M. & Koh, C. G. (2011). Hydroelastic response of very large floating structure with a flexible line connection. *Ocean Engineering, 38*, 1957−1966. https://doi.org/10.1016/j.oceaneng.2011.09.021

Nam, B. W., & Hong, S. Y. (2021). Eigenvalue analysis for motion response of a TLP and tender semi considering a complex mooring configuration. *International Journal of Offshore and Polar Engineering, 31*(2),169−177. https://doi.org/10.17736/ijope.2021.mm26

Zhang, H., Xu, D., Xia, S., Qi, E., Tian, C., & Wu, Y. (2015). Nonlinear network dynamic characteristics of mulit-module floating airport with flexible connectors. *Proceedings of the Twenty-fifth International Ocean and Polar Engineering Conference*, Kona, Hawaii, USA, 1583−1590.

Otto, W. J., Waals, O. J., Bunnik, T., & Ceneray, C. (2019a). Wave induced motions of a floating mega island. In: Wang, C., Lim, S., & Tay, Z. (Eds.), *WCFS2019, Lecture notes in civil engineering: Vol. 41.* (pp. 173−189). Springer. https://doi.org/10.1007/978-981-13-8743-2_9

Otto, W. J., Waals, O. J., Bunnik, T. H. J., & Cresp, J. (2019b). Optimization of wave induced motions and forces on a floating island. *Proceedings of the Twenty-ninth International Ocean and Polar Engineering Conference*, Honolulu, Hawaii, USA, 3120−3126.

Waals, O.J ., Bunnik, T. H .J., & Otto, W. J. (2018). Model tests and numerical analysis for a floating mega island. *Proceedings of the 37th International Conference on Ocean. Offshore and Arctic Engineering*, Madrid, Spain. V001T01A016. https://doi.org/10.1115/OMAE2018-78589

Zalar, M., Diebold, L., Baudin, E., Henry, J., & Chen, X. -B. (2007). Sloshing effects accounting for dynamic coupling between vessel and tank liquid Motion. *Proceedings of the 26th International Conference on Offshore Mechanics and Arctic Engineering*, San Diego, USA, 687−701. https://doi.org/10.1115/OMAE2007-29544

Wu, Y., Wang, D., Riggs, H. R., & Ertekin, R. C. (1993). Composite singularity distribution method with application to hydroelasticity. *Marine Structures, 6*(2-3), 143−163. https://doi.org/10.1016/0951-8339(93)90017-W

Choi, Y. R., & Hong, S. Y. (2002). An analysis of hydrodynamic interaction of floating multi-body using higher-order boundary element method. P*roceedings of the Twelfth International Offshore and Polar Engineering Conference. *Kitakyushu, Japan, 303−308.

Author ORCIDs

Author name	ORCID
Park, Hyo-Jin	0000-0002-6491-6400
Kim, Jeong-Seok	0000-0002-0416-4403
Nam, Bo Woo	0000-0003-1125-7453